Computers & Structures Vol. 37, No. 6, pp. 1105–1116, 1990
Printed in Great Britain.

0045-7949/90 $3.00 + 0.00

FINITE ELEMENT ANALYSIS OF THE SHEAR VANE TEST

D. V. GRIFFITHS and P. A. LANE
Department of Engineering, University of Manchester, Manchester M13 9PL, U.K.

(*Received* 30 *January* 1990)

Abstract—Finite element analyses of the standard shear vane test to measure the *in situ* undrained shear strength of soil are presented. The mobilization of shear stresses on the vertical and horizontal faces of the vane has been studied up to failure and compared with analytical solutions. This has been achieved by the use of 2-D and quasi-3-D analyses. Good agreement between the computed and analytical solutions was achieved provided the soil strength was isotropic. The influence of soil strength anisotropy was considered by the use of a simple model in which the undrained shear strength was related to direction. The effect of strain softening was also incorporated into the analyses. When combined with the quasi-3-D analysis, these features allowed more realistic models to be made of the shear strength mobilization on all parts of the cylindrical failure surface.

NOTATION

c_u	undrained shear strength
$c_{u,r}$	undrained shear strength on top or bottom surfaces
$c_{u,z}$	undrained shear strength on side surfaces
$c_{u,\alpha}$	undrained shear strength at an inclination of α to the vertical
$c_{u,\text{peak}}$	peak undrained shear strength in a softening material
$c_{u,\text{res}}$	residual undrained shear strength in a softening material
$c_{u,\text{vane}}$	undrained shear strength 'in the mass'
D	diameter of vane
f	anisotropy factor
G	elastic shear modulus
H	height of vane
H'	gradient of softening curve
R	radius of vane
T_h	torsional resistance on sides of vane
T_v	torsional resistance on top or bottom of vane
T_{vane}	peak torsional resistance of vane as would be measured in field
α	inclination to vertical of peak shear stress
β	scalar ratio of radius R
θ	angular position around vane circumference
$\bar{\varepsilon}$, $\bar{\sigma}$	strain and stress invariants
σ_r, σ_z, τ_{rz}	stresses in the r–z-plane

1. INTRODUCTION

The estimation of the *in situ* undrained shear strength of a soft clay from the response of a standard shear vane test is an important part of geotechnical site investigation. The simplified equations which describe the shear experienced by the vertical and horizontal faces of the standard vane (Fig. 1) are based on assumptions about the distribution of shear stresses on these faces and the failure mode of the vane in the soil. The investigation described here seeks to investigate the legitimacy of these assumptions and to comment on features affecting the test which may be accounted for by the use of semi-analytical multiplying factors (see e.g. [1–3]).

The propagation of the shear surface from the tips of the vane when subjected to an applied torque was initially studied using a plane strain model. This 2-D model accounted only for shear resistance developed at the sides of the vane as it is twisted in the ground. Following these analyses, a quasi-3-D approach is described which uses a Fourier series to model variations in the tangential directions [4–8]. This semi-analytical approach allowed observations to be made of the distribution and mobilization of shear stresses on the sides and top (bottom) of the vane. This quasi-3-D approach is attractive because it allows many of the important 3-D features to be accounted for without the considerable computational time and storage required by a full 3-D non-linear finite element analysis.

The assumed distribution of shear stresses on the vane faces and ends is usually simplified to allow an estimation of the resultant torque. The maximum torque experienced on the side surfaces of a standard shear vane (height H, diameter D) in a soil of undrained shear strength c_u is given by

$$T_v = \frac{\pi D^2 H c_u}{2}, \tag{1}$$

assuming a rectangular distribution of shear stresses at the sides (Fig. 2).

The maximum torque experienced on the top and bottom surfaces of a standard shear vane is

$$T_h = \frac{\pi D^3 c_u}{6}, \tag{2}$$

assuming a rectangular distribution (Fig. 3a), and

$$T_h = \frac{\pi D^3 c_u}{8}, \tag{3}$$

assuming a triangular distribution (Fig. 3b).

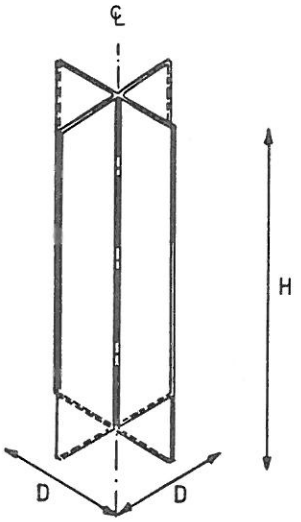

Fig. 1. Standard shear vane.

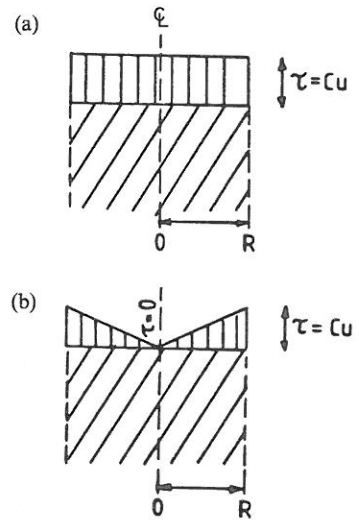

Fig. 3. (a) Rectangular and (b) triangular shear stress distributions at failure on the top.

All three equations assume that the shear stresses generated on each blade face are then mobilized over the surfaces of a cylinder of height H and diameter D (Fig. 4).

The maximum torque registered by the vane is then

$$T_{\text{vane}} = T_v + T_h \tag{4}$$

if both contributory torques are fully mobilized, taking account of both the top and bottom shear surfaces. One of the aims of this paper is to determine which of eqns (2) or (3) is more appropriate for use in eqn (4). It is likely that because of progressive failure of the soil surrounding the vane, not all shear stresses will reach their limit simultaneously. In addition, at large strains, the soil may become remoulded and weaken to a residual value of undrained strength, which would be reflected in a reduced torque measured at ground level. These features will also be investigated in this work.

Relatively little finite element analysis has been reported on the shear vane test, probably because of the three-dimensionality of the problem. Donald *et al.* [9] presented elastic stress distributions on the vane face and ends using solid eight-node brick finite elements. They tested two clays with vanes of different sizes to estimate the face and end torques, and it was noted that the torques on the two surfaces were mobilized at different strain levels. In the present work, particular attention is paid to eqns (1)–(3), and their underlying assumptions in dealing with the effects of progressive failure, stress mobilization and strain softening in the analysis of vane test results.

All the analyses described in this paper assume that

(1) rate effects are not important,
(2) the blades are perfectly rough,
(3) there is no separation from the soil at the back of the vane blades,
(4) the area of influence is not greater than three vane radii from the vane axis, and
(5) the soil is adequately modelled as an elastic/perfectly plastic (von Mises) material.

The purpose of this work is to present, for the first time, nonlinear analyses of the shear vane test using

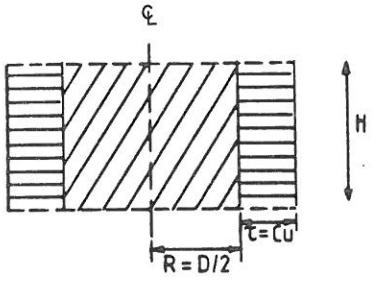

Fig. 2. Shear stress distribution at failure on the sides.

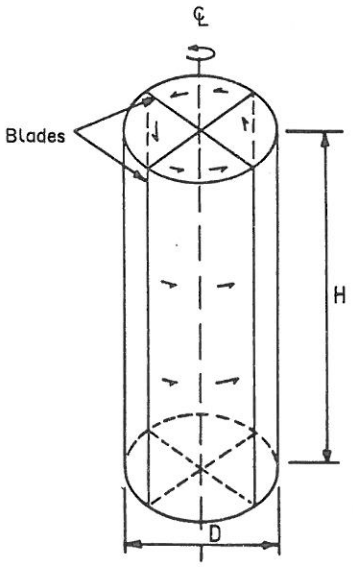

Fig. 4. Circumscribing cylinder of shearing surfaces.

relatively simple constitutive models and numerical finite element procedures. As will be described, the quasi-3-D approach allows many of the important features of the shear vane to be reproduced numerically without resorting to a full 3-D analysis. The chief disadvantage is that the vane must be modelled as a solid cylinder.

The results presented are qualititive in nature, with priority given to the observation of relative rates of mobilization of shear stresses on the different failure surfaces. Realistic values of the soil's elastic properties before failure have not been considered of prime importance for modelling failure conditions.

2. 2-D ANALYSES

A plane strain mesh of eight-node quadrilateral elements was used with an elastic, perfectly plastic (von Mises) soil model for the 2-D analysis. The analyses used an elasto-viscoplastic algorithm (see e.g. [10]). The problem was modelled as a horizontal slice of soil of unit depth, surrounding an infinitely long vane. The mesh was designed so that the majority of finite elements occurred at the positions of greatest shear stress gradients, namely the blade ends. As a result of symmetry, only a quarter of the problem was modelled. Figure 5 shows the mesh which represents a plan view of the soil. The blades themselves were modelled by applying prescribed displacements to the appropriate boundary nodes, which increased linearly from zero at the centre to a maximum at the tip. The boundary conditions assumed in Fig. 5 were such that only tangential movement was allowed at the tips of the vane blades. This was considered to be consistent with a material which exhibits no volume change during shear.

The torque at any stage was back-figured from the reaction forces acting at the displaced nodes, which in turn were calculated from the Gauss-point stresses once equilibrium and yield were satisfied.

The development of the computed torque with tip rotation is shown in Fig. 6, and compared with the result of eqn (1). The finite element result exceeded the simple analytical result by less than 3%. Figures 7 and 8 show displacement vectors and the deformed mesh for this case, confirming the rather localized mechanism that is formed around the vane circumference. To investigate the effects of progressive failure, Fig. 9 shows the shear stresses mobilized at a point near the blade edge and one at the same radius but at 45° to the blades. The figure shows that soil adjacent to the vane is first to reach failure, followed by soil midway between the blades, which requires approximately twice as much angular displacement to reach failure conditions.

3. QUASI-3-D ANALYSES

The 2-D analyses confirmed the localized nature of the cylindrical failure mechanism for the vane in the soil. The 2-D analyses, however, have no information about the mobilization of shear stresses on the top and bottom surfaces of the vane. In an attempt to model the 'full' problem, a quasi-3-D approach is

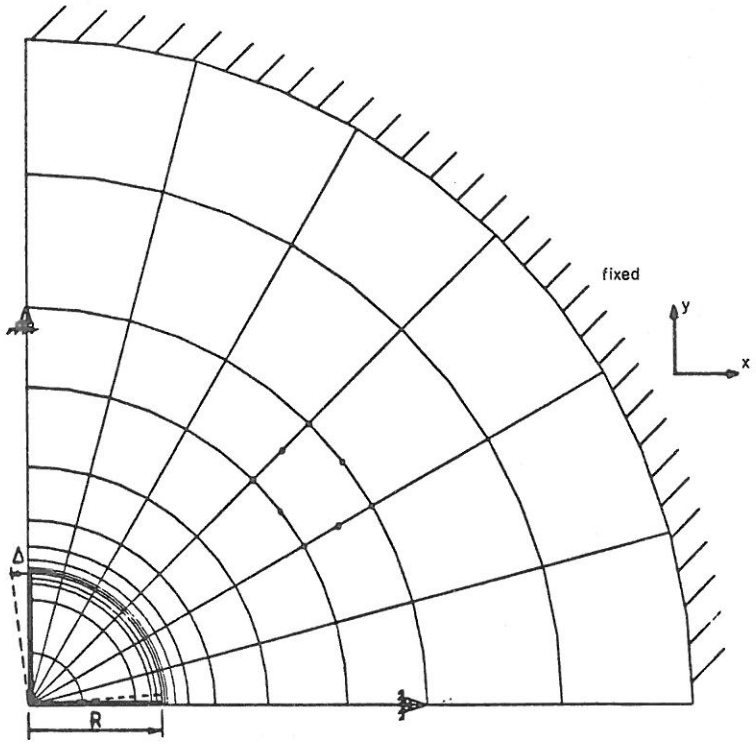

Fig. 5. The 2-D mesh and boundary conditions.

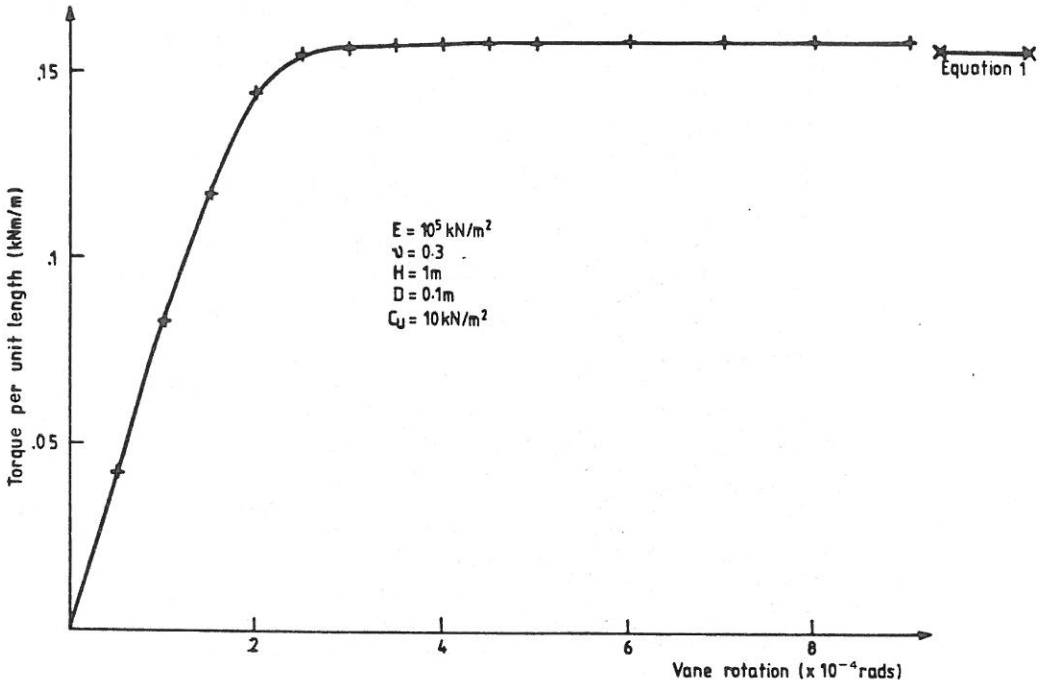

Fig. 6. Torque vs angular rotation (2-D analysis).

used. This method is suitable for axisymmetric bodies subjected to non-axisymmetric loading, and has been used previously by the authors for problems of this type [7, 8]. Although the vane is not an axisymmetric body, the cylindrical failure surface confirmed by the 2-D analyses does fall into this category. Hence in the quasi-3-D approach the vane is replaced by a solid cylinder of stiff material which will be rotated into the soil. It is true that this approximation predetermines the failure surfaces, but the method will allow relatively simple analyses to be performed which will indicate the way in which shear stresses are mobilized over all of the cylinder's surfaces.

The method requires only a 2-D mesh to be formed in the r–z-plane, as shown in Fig. 10. Two axes of symmetry are indicated, one on the axis of rotation

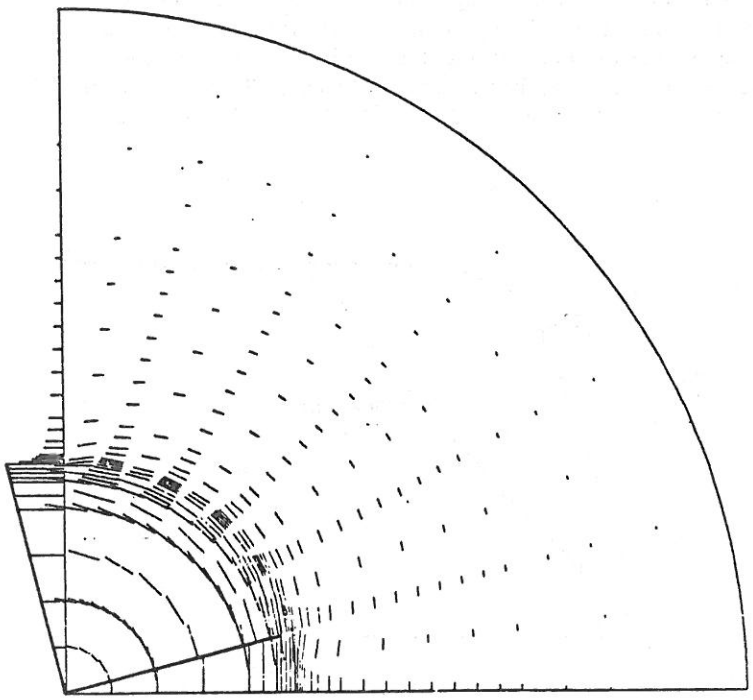

Fig. 7. Displacement vectors at failure.

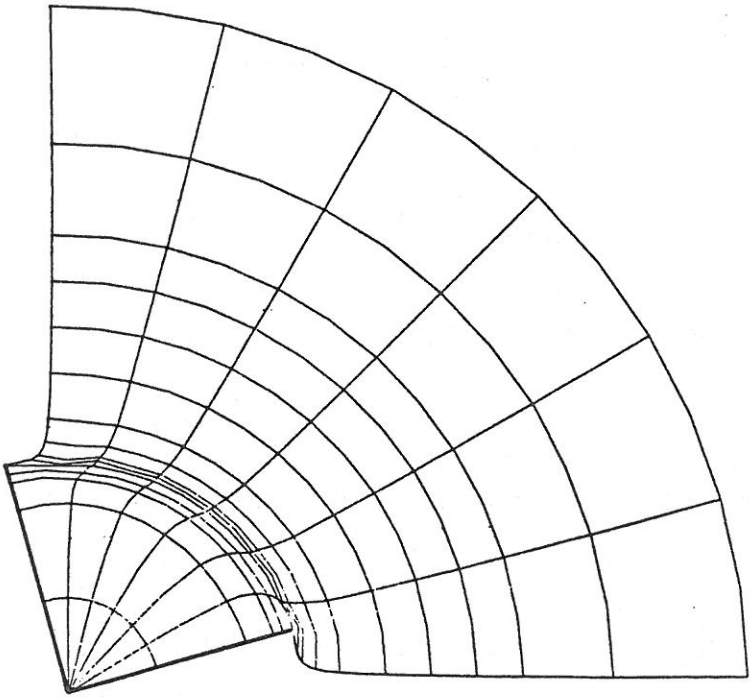

Fig. 8. Deformed mesh at failure.

of the vane and one at the mid-height of the vane. The boundary conditions permit rotational freedoms only on the axis of rotation, with vertical movement suppressed on the mid-height axis. In addition, vertical movement is not allowed on the top surface of the mesh, implying that the vane is embedded at considerable depth; this avoids any complications caused by proximity of the ground surface.

All stresses, strains and displacements in tangential directions are modelled semi-analytically by expansions of a Fourier series. For torsional loading, the situation is simplified because no tangential variations occur and only one harmonic in the series is required [11]. This leads to significant savings in computer time and storage requirements.

Initially an elastic analysis was performed for a typical angular rotation of the cylinder. Figure 11 shows the elastic distribution of shear stresses on the top and side of the cylinder. The shape of the distributions, including the corner peaks and the rapid fall in stress away from the edges, was noted by Chandler [2] and Donald *et al.* [9].

In the elastic/plastic case using the same properties as before, the cylinder is rotated in the soil and failure is reached first at the corner of the vane, as suggested by Fig. 11. Further rotation causes the failure surface

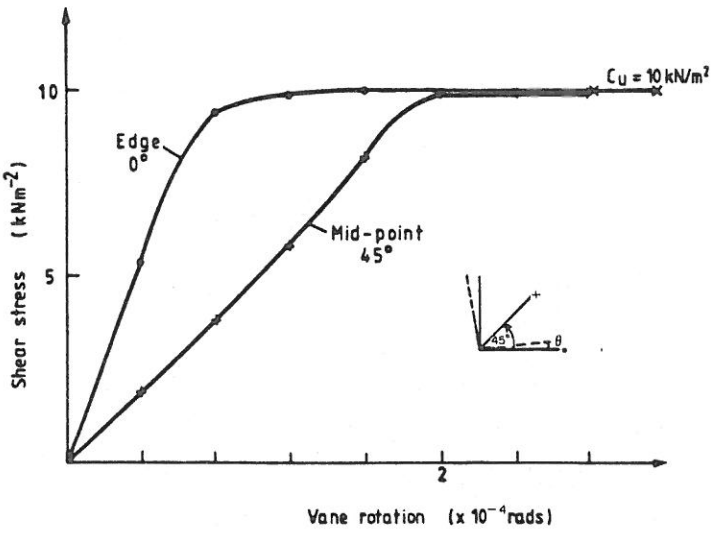

Fig. 9. Variations in the rate of shear stress mobilization.

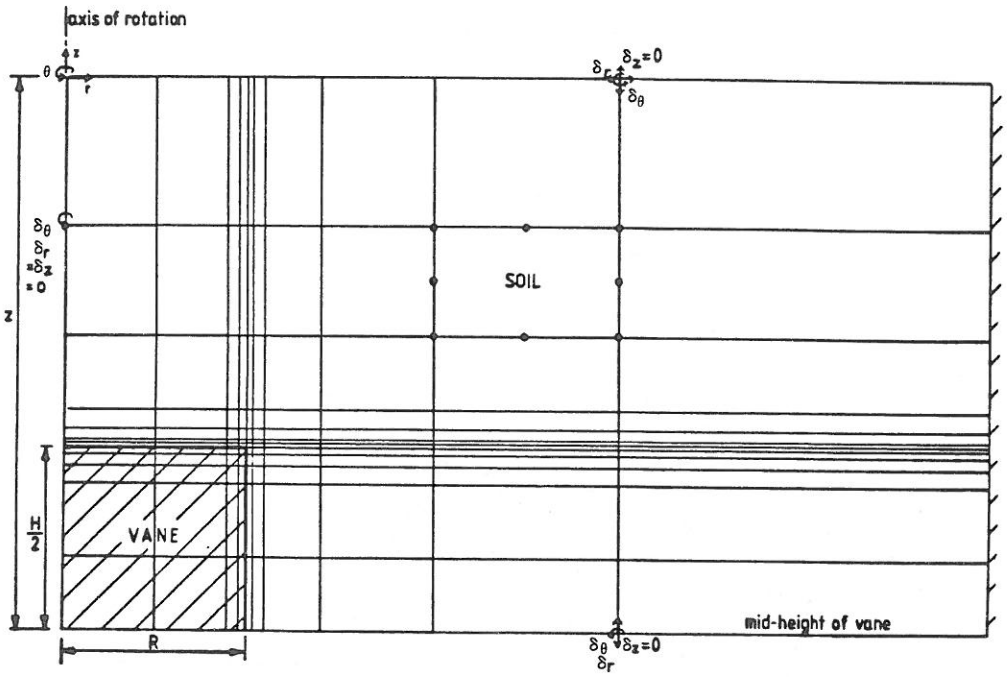

Fig. 10. Quasi-3-D mesh and boundary conditions.

to spread down the side of the vane and in towards the axis of rotation. The situation close to peak torque is shown in Fig. 12. It would appear that although the full shear strength is readily mobilized at the sides of the vane, this does not occur at the top or bottom because of the very small strains experienced close to the axis of rotation. The shear stress distribution at the top certainly exceeds the triangular distribution (Fig. 3b), but never quite reaches the rectangular distribution (Fig. 3a), because of the singularity at the axis of rotation.

Figure 13 shows the build-up of torque on the top and side surfaces. As expected, the contribution from the top and bottom surface requires larger strains to be 'fully' mobilized as compared with torque from the

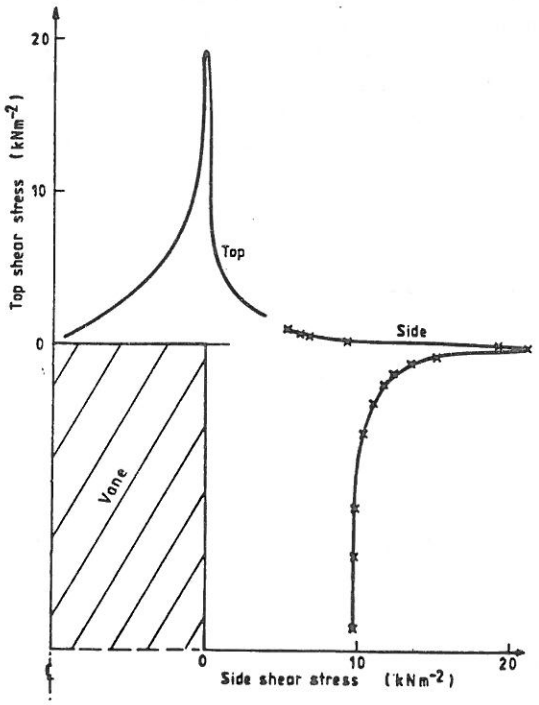

Fig. 11. Elastic distribution of shear stress on sides and top of vane.

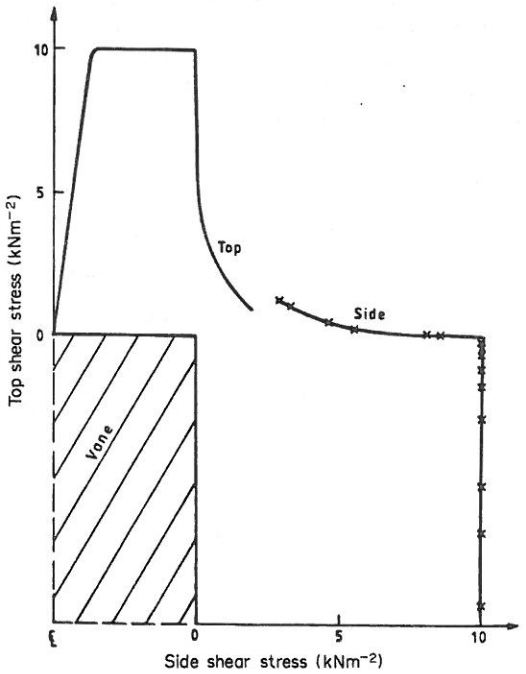

Fig. 12. Elasto-plastic distribution of shear stress on sides and top of vane close to failure.

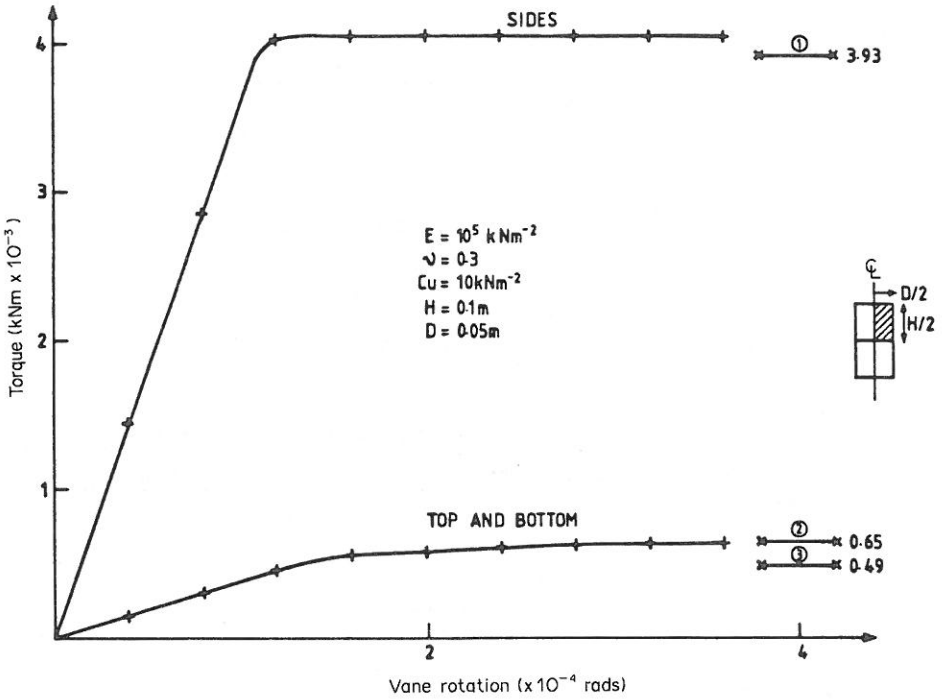

Fig. 13. Torque on sides and top vs angular rotation in isotropic soil.

sides. The torque coming from the side resistance is again less than 3% greater than that given by eqn (1). The torque coming from the top and bottom surface lies between the rectangular and triangular solutions of eqns (2) and (3) respectively.

In view of the distribution of shear stress observed on the top (or bottom) surface of the vane, it might be justified to represent this shape as a combination of a triangle and a rectangle. The triangle would vary from zero at the axis of rotation to c_u at a radius of βR. The rectangle would have a constant height of c_u between radii of βR and R. According to Fig. 12, $\beta \approx 0.3$; however, the contribution to torque from this triangular area would be insignificant. Thus the rectangular solution of eqn (2) seems the most realistic in this case.

Chandler [2] suggested that the true divisor from eqns (2) and (3) to give the combined torque from the top and bottom surfaces should lie between six and eight. The present result suggests that for isotropic soils the divisor should be put equal to six. Not only does this give closer agreement with the computed values, but it also leads to a conservative lower-bound on the value of c_u.

4. SOIL ANISOTROPY

If a soil's strength is a function of direction, this will clearly influence the result in a vane test where the main shearing surfaces are at right angles to each other. In this problem, the directions of the maximum shear stress coincide with the physical boundaries of the vane, namely on the top, bottom and sides of the shearing surface.

A simple model is proposed [11] which allows the undrained shear strength c_u to vary as a function of the angle α (in degrees), where α is the inclination of the maximum shear stress to the vertical direction; thus

$$\alpha = \tfrac{1}{2}\tan^{-1}\frac{2\tau_{rz}}{\sigma_r - \sigma_z} + 45^\circ, \tag{5}$$

where σ_r, σ_z and τ_{rz} are the stresses in any radial plane.

Once α is found, the value of c_u at that inclination is given by

$$c_{u\alpha} = c_{uz}\left(1 + \frac{\alpha}{90^\circ}(f-1)\right), \tag{6}$$

where f is an anisotropy factor, defined as

$$f = \frac{c_{ur}}{c_{uz}}, \tag{7}$$

and c_{ur} and c_{uz} are the undrained shear strengths on the top and side surfaces respectively.

Using the quasi-3-D approach, an anisotropic soil was analysed in which $c_{uz} = 15\ \text{kN/m}^2$ and $c_{ur} = 10\ \text{kN/m}^2$ ($f = 2/3$). As shown in Fig. 14, the two components of torque are closely reproduced to the same levels of accuracy as obtained for isotropic soils.

Although the model described by eqns (5)–(7) allows for a gradual change in c_u with direction, the result suggests that this transition is unimportant as the solution is dominated by the top, bottom and side values.

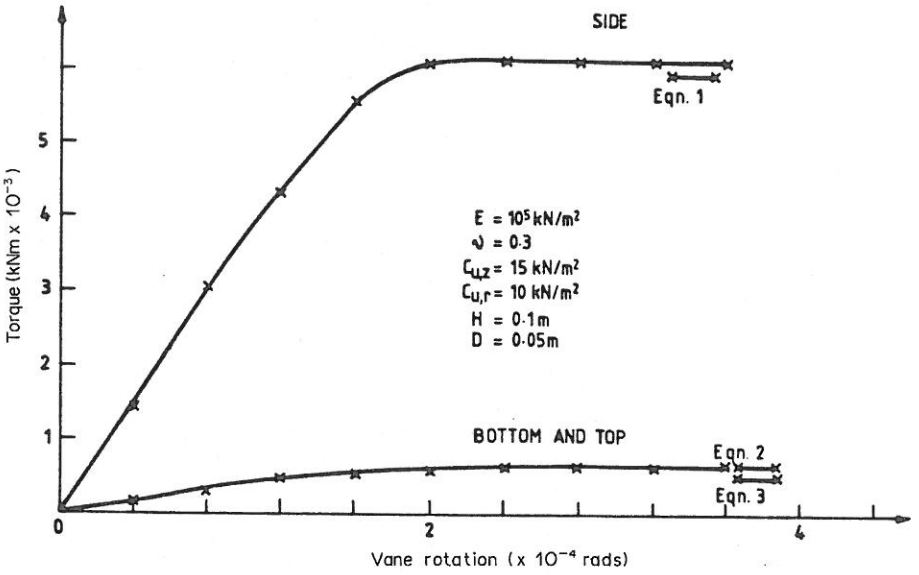

Fig. 14. Torque on sides and top vs angular rotation in anisotropic soil.

5. STRAIN SOFTENING

As a shear vane is twisted in the ground, it is likely that remoulding of the soil will result in softening of the undrained shear strength once a peak value has been mobilized. This type of progressive failure may have a significant effect on the measured torque and hence the value of c_u that would be backfigured from eqn (4).

In this section, a simple softening model is introduced into the finite element analyses. The method takes account of the variation in c_u by means of the stress and strain invariants [12]:

$$\bar{\sigma} = \frac{1}{\sqrt{2}}[(\sigma_r - \sigma_z)^2 + (\sigma_z - \sigma_\theta)^2 + (\sigma_\theta - \sigma_r)^2 + 6(\tau_{rz}^2 + \tau_{z\theta}^2 + \tau_{\theta r}^2)]^{\frac{1}{2}} \quad (8)$$

$$\bar{\varepsilon} = \frac{\sqrt{2}}{3}[(\varepsilon_r - \varepsilon_z)^2 + (\varepsilon_z - \varepsilon_\theta)^2 + (\varepsilon_\theta - \varepsilon_r)^2 + \tfrac{3}{2}(\gamma_{rz}^2 + \gamma_{z\theta}^2 + \gamma_{\theta r}^2)]^{\frac{1}{2}}. \quad (9)$$

The stress–strain relationship is assumed to be of the form given in Fig. 15, and the gradients of the elastic (hardening) and plastic (softening) portions are given by:

$$\frac{\bar{\sigma}}{\bar{\varepsilon}} = 3G, \quad \text{in plane strain} \quad (10)$$

and

$$\frac{\bar{\sigma}}{\bar{\varepsilon}} = H' \quad (11)$$

respectively, where G is the elastic shear modulus and $H'/3G$ is a 'brittleness' parameter which equals zero

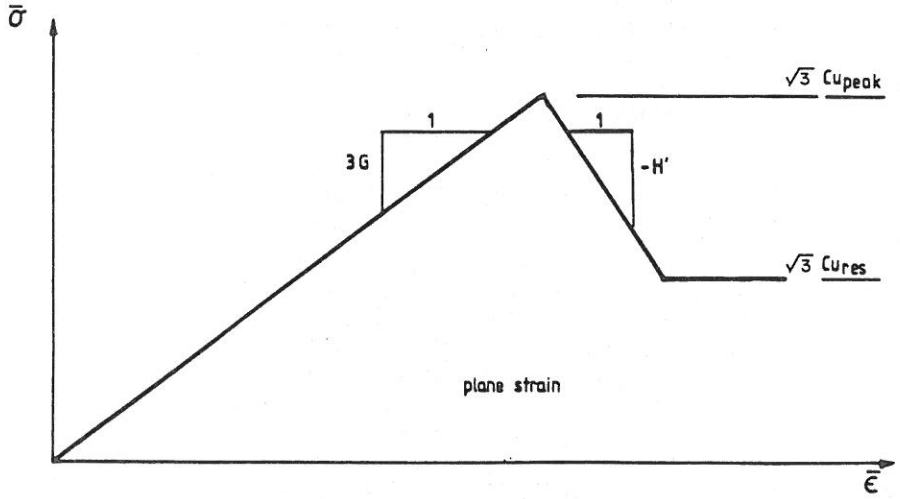

Fig. 15. Definition of terms in softening model (2-D analysis).

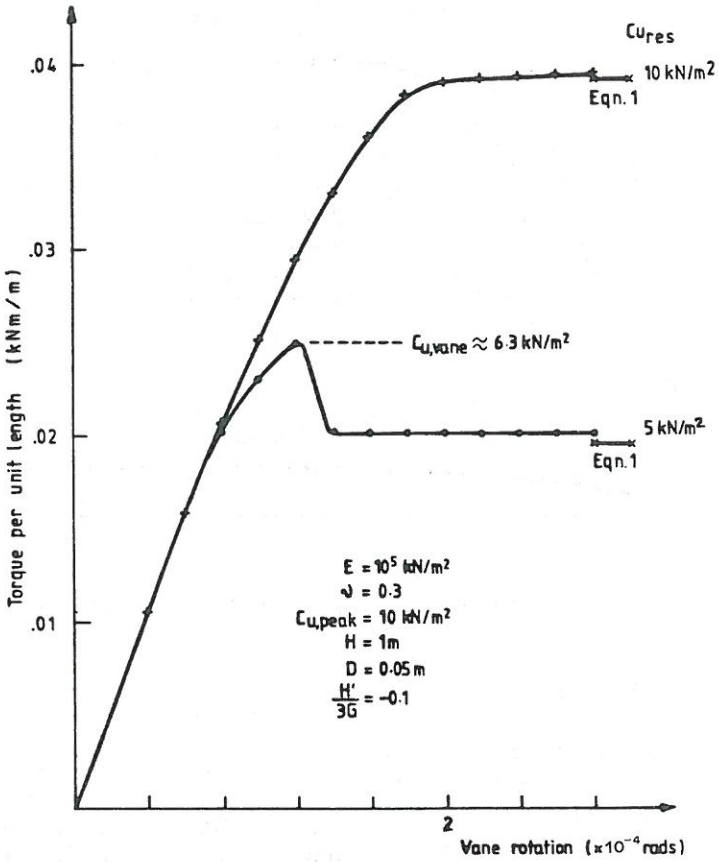

Fig. 16. Torque vs angular rotation in softening and non-softening soil (2-D analysis).

for perfectly plastic behaviour. Thus, the model remains elastic until the peak strength $c_{u,\text{peak}}$ is mobilized, followed by softening at a rate given by H' until a residual strength $c_{u,\text{res}}$ is reached.

Figure 16 gives the effect on the measured side torque of a 50% reduction in c_u from its peak to residual values in the 2-D model. The rate of softening in this case was given by $H'/3G = -0.1$. Because of progressive failure in the soil, the maximum torque possible with $c_{u,\text{peak}}$ is not reached before softening reduces the torsional resistance. If an estimate of the undrained strength of the soil was made from this result, a value of $c_{u,\text{vane}}$ 'in the mass' would be obtained, where

$$c_{u,\text{res}} < c_{u,\text{vane}} < c_{u,\text{peak}}. \tag{12}$$

In the example of Fig. 16 where $c_{u,\text{peak}} = 10\ \text{kN/m}^2$ and $c_{u,\text{res}} = 5\ \text{kN/m}^2$, the value of $c_{u,\text{vane}}$ that would be back-figured from the maximum torque is approximately $6.3\ \text{kN/m}^2$. Eventually, the residual torque corresponding to $c_{u,\text{res}}$ is reached and has the same degree of accuracy as obtained with previous non-softening results.

The variation in mobilized shear strength at a constant vane-tip radius for different amounts of vane rotation in the 2-D analyses is shown in Fig. 17. The progressive nature of shear stress mobilization is clearly seen. In the perfectly plastic case, failure is first reached at the vane tips and gradually spreads to points between the blades. Eventually, all points reach the fully mobilized shear strength (in this case $10\ \text{kN/m}^2$).

In the softening case, the soil at the vane tips reaches peak strength and starts to soften towards the residual value. This softening in the vicinity of the vane tips occurs while soil between the blades is still climbing towards the peak. Eventually, all points pass through the peak and soften towards the residual value (in this case $5\ \text{kN/m}^2$). A very gentle softening slope of $H'/3G = -0.01$ was used to obtain the results shown in Fig. 17. Curve 5 gives the situation where all points have reached residual except a small zone exactly halfway between the blades. In an actual field vane, separation occurs at the back of the blade face (see e.g. [3]), reducing the rate of development of shear stress and increasing the effect of progressive failure further.

Progressive failure is particularly apparent across the top of the vane, and the use of the quasi-3-D model allows this to be seen. Figure 18 gives the development of shear stress down the side of the vane and across the top with increasing strain. This figure includes both strain softening and anisotropy in that $c_{u,\text{peak}}$ and $c_{u,\text{res}}$ are different for the sides and top

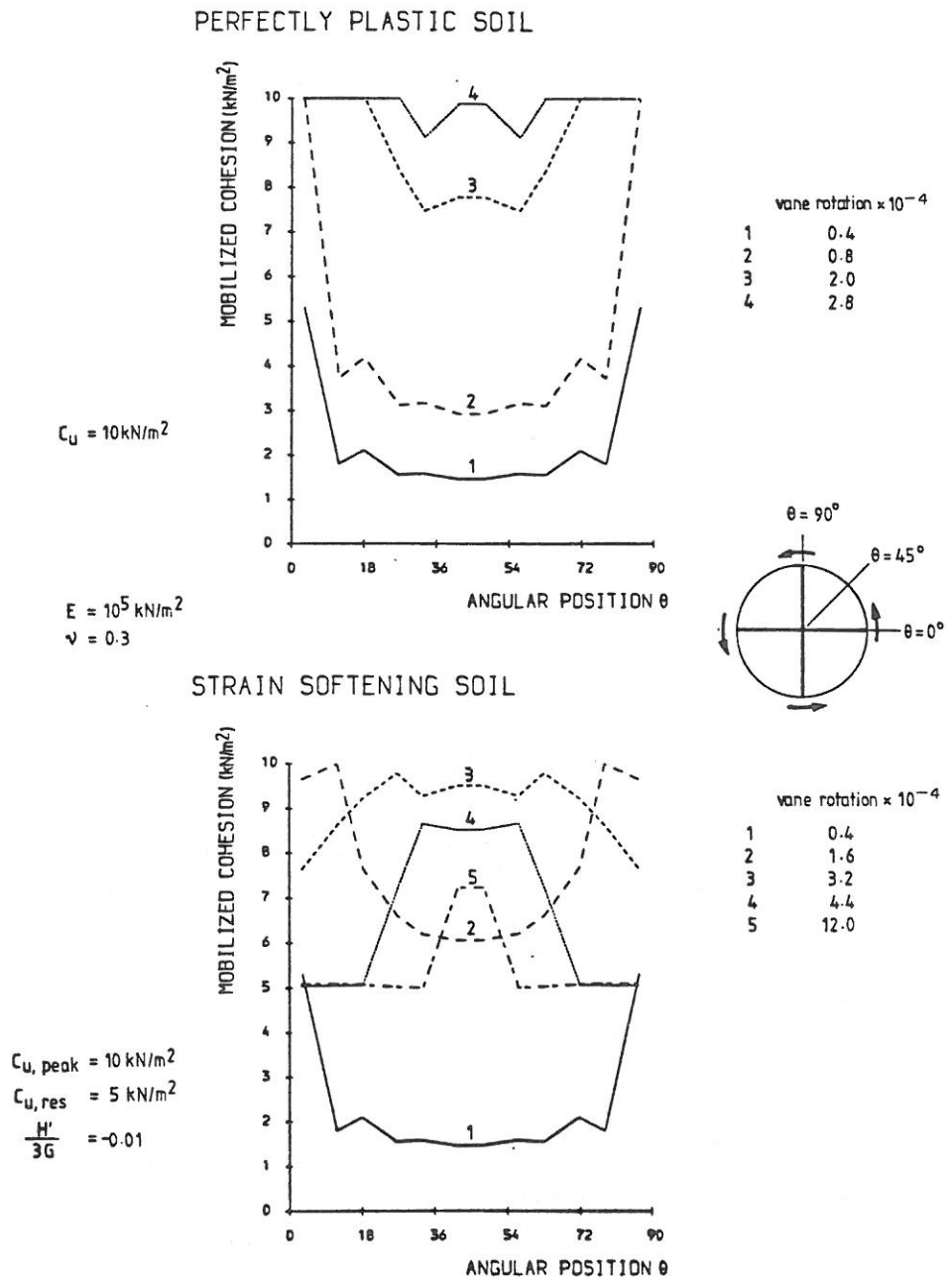

Fig. 17. Mobilization of shear stress around the vane circumference.

surfaces. Remoulding of soil is seen initially at the vane corners and gradually spreads towards the centre. As remoulding spreads along the top surface, the residual torque for the whole vane is gradually reached, as would be measured in the field by a test taken to large strains.

Figure 19 shows the effects of combining strain softening with anisotropy together with various degrees of post-peak 'brittleness' by varying H'. The maximum torque response is reduced with increasing 'brittleness', but the residual torque is unaffected.

6. CONCLUSIONS

Both 2-D and quasi-3-D finite element analyses of the shear vane test have been performed, to allow the mobilization of shear stresses on the failure surfaces to be monitored. The conventional formulae for the mobilization of shear stresses have been shown to be acceptable for isotropic, non-softening materials, with the peak shear stress distribution on the vane ends adequately modelled using a rectangular assumption. For more realistic analysis of the vane test, anisotropy and strain softening were also considered. The

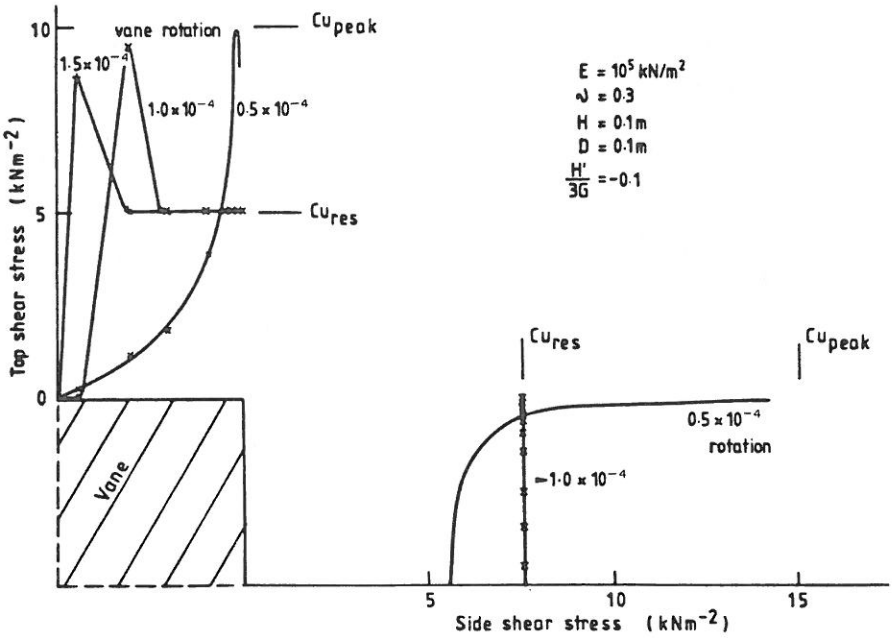

Fig. 18. Progressive failure on top and sides in anisotropic soil with softening.

modelling of strain softening showed the effects of progressive failure and the propagation of residual strength conditions. Strain softening in a soil deposit remains a difficult phenomenon to measure in any rigorous way. The shear vane test can measure the residual strength of the soil with some confidence, however, the value of $c_{u,\text{vane}}$ 'in the mass' computed from the maximum torque measured in a softening soil can only represent a lower bound on the actual peak strength.

Acknowledgements—P. A. Lane has been sponsored by the Science and Engineering Research Council for the duration of her research at Manchester University. Development of the HARMONY program was supported in part by Fugro Geotechnical Engineers, P.O. Box 63, Leidschendam, The Netherlands.

REFERENCES

1. G. Aas, A study of the effect of vane shape and rate of strain on the measured values of *in situ* shear strength

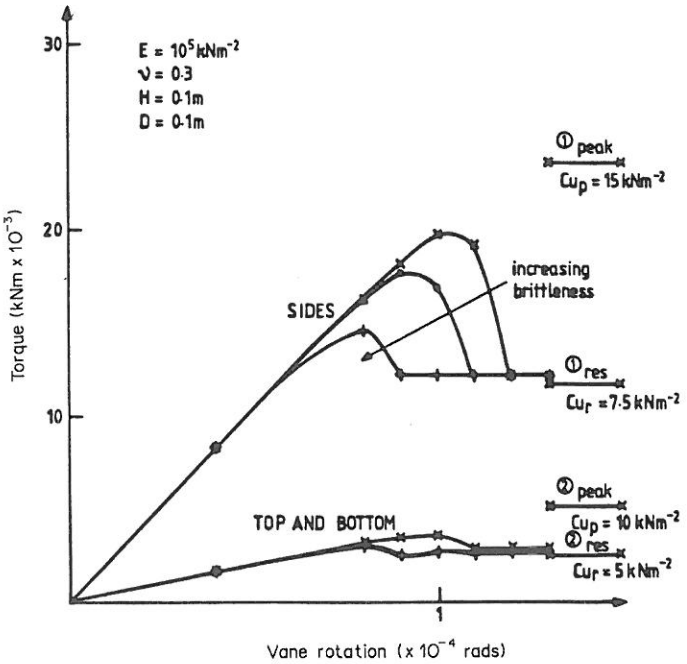

Fig. 19. Torque vs angular rotation showing effects of 'brittleness' on peak value.

of clays. *Proc. 6th Int. Conf. Soil Mechanics and Foundation Engineering*, pp. 141–145 (1965).
2. R. J. Chandler, The *in situ* measurement of undrained shear strength using the field vane test. *Int. Symp. Laboratory and Field Vane Strength Testing*, American Society for Material Testing, Tampa, FL (1987).
3. C. M. Merrifield, Factors affecting the interpretation of the *in situ* shear vane test. Ph.D. Thesis, Department of Civil Engineering, University of Surrey (1980).
4. E. L. Wilson, Structural analysis of axisymmetric solids. *J. Am. Inst. Aeronaut. Astronaut.* **3,** 2269–2274 (1965).
5. O. C. Zienkiewicz, *The Finite Element Method*, 3rd Edn. McGraw–Hill, London (1977).
6. L. A. Winnicki and O. C. Zienkiewicz, Plastic behaviour of axisymmetric bodies subjected to non-axisymmetric loading. *Int. J. Numer. Meth. Engng* **14,** 1399–1412 (1977).
7. D. V. Griffiths, HARMONY—a program for predicting the response of axisymmetric bodies subjected to non-axisymmetric loading. Technical Report, Department of Engineering, University of Manchester (1985).
8. D. V. Griffiths and P. A. Lane, The influence of interface roughness on problems of axisymmetric soil/structure interaction. In *Proc. 2nd Int. Conf. Constitutive Laws for Engineering Materials* (Edited by C. S. Desai, E. Krempl, P. D. Kiousis and T. Kundu), pp. 1051–1058. Elsevier, Amsterdam (1987).
9. I. B. Donald, D. O. Jordan, R. J. Parker and C. T. Toh, The vane test—a critical appraisal. *Proc. 9th Int. Conf. Soil Mechanics and Foundation Engineering*, pp. 81–88 (1977).
10. I. M. Smith and D. V. Griffiths, *Programming the Finite Element Method*, 2nd Edn. John Wiley, Chichester (1988).
11. P. A. Lane, Finite element analysis of axisymmetric and non-axisymmetric problems in geomechanics. Ph.D. Thesis, Department of Civil Engineering, University of Manchester (1990).
12. D. V. Griffiths, Computation of strain softening behaviour. In *Proc. Symp. Implementation of Computer Procedures and Stress–Strain Laws in Geotechnical Engineering* (Edited by C. S. Desai and S. K. Saxena), pp. 591–604. Acorn Press, Durham, NC (1981).